Proc. Natl. Acad. Sci. USA
Vol. 91, pp. 12388–12392, December 1994
Biophysics

Stereospecific dihaloalkane binding in a pH-sensitive cavity in cubic insulin crystals

(anesthetic–protein interactions/water polarization/carboxyl group pairing/allostery)

OLGA GURSKY†, ERIC FONTANO‡, BALAJI BHYRAVBHATLA‡, AND DONALD L. D. CASPAR‡

Rosenstiel Basic Medical Sciences Research Center, Brandeis University, Waltham MA 02254-9110

Contributed by Donald L. D. Caspar, July 29, 1994

ABSTRACT **Crystallographic analysis at 2-Å resolution of the selective binding of dihalogenated methane, ethane, and ethylene compounds in the cavity on the cubic insulin dimer axis provides a model for anesthetic–protein interactions. At pH 6–11, 1,2-dichloroethane binds isomorphically in the right-handed cis-conformation, displacing four water molecules from the invariant cavity. Lowering the pH to 5.7 in 1 M Na_2SO_4 without dihaloalkanes induces a cooperative structural transition in which the dyad cavities between B13 glutamate pairs are constricted, and SO_4^{2-} ions are bound by rearranged triads of B1 NH_3^+ groups. In the presence of dichloroethane at pH 5–5.5, the equilibrium is shifted to a mixture of the ligand-bound and ligand-excluding cavity structures, with half-occupancy of the sulfate sites, exemplifying how a volatile anesthetic can act as an allosteric effector. Measurements at pH 9 of the occupancies of structurally similar dihaloalkanes demonstrate a high degree of binding selectivity. Induced polarization of the ligand and bound water by the charge distribution in the binding cavity apparently provides the selective electrostatic interactions that discriminate between dihaloalkanes of comparable size and polarity.**

Insulin (51 amino acids, 5.8 kDa) crystallizes from zinc-free alkaline solutions as a symmetric dimer arranged in orthogonal cross-connected rows in the cubic space group $I2_13$ (a = 78.9 Å) (1, 2). The crystal lattice, which contains 65% solvent volume, is stable from pH 7–10 in 0.1 M monovalent cation salt solutions (3) and from pH 5–11 in 1 M Na_2SO_4. The pH-dependent local conformational changes and coupled binding of monovalent cations, which have been crystallographically characterized in pH range 7–11 (4), demonstrate the usefulness of this system for studying the effects of altered electrostatic interactions on the protein and solvent structure. Following our observation (4) that cubic insulin crystals in alkaline 0.1–1 M salt solutions bind 1,2-dichloroethane ($ClH_2C—CH_2Cl$) with unit occupancy at a site on the dimer axis (Fig. 1), we have characterized this binding at pH 5–11 and compared the binding of similar dihaloalkanes at pH 9.§ Such binding exemplifies the type of hydrophobic ligand–protein interactions that may underlie the action of inhalational general anesthetics (6, 7).

MATERIALS AND METHODS

Crystal Preparation and X-Ray Data Collection. Cubic Zn-free crystals of bovine insulin, grown from phosphate buffer at pH 9 (1, 4), were equilibrated by dialysis against sodium salt solutions that varied in pH from 5 to 11 and subsequently equilibrated with liquid dihaloalkanes. Dihaloalkane binding was discovered by exposing the crystals to 1,2-dichloroethane as solvent for Formvar, which was applied in the capillary to cast an encasing film that prevents crystal slippage (8). Binding at the dyad site, as detected by x-ray diffraction, was complete after 30-sec direct exposure to liquid dichloroethane or after overnight soaking in a saturated aqueous solution. The x-ray data were collected using the Brandeis television area detector (9) or charge-coupled device area detector (10) with Cu K_α radiation from an Elliott rotating anode generator. The data were processed using the MADNES program (11), and intensities were obtained by three-dimensional profile fitting with subsequent radiation and absorption corrections (12). For each experimental condition tested, the data sets (usually collected from two or three crystals) were reproducible with scaling R-factors of 8–11%. The data from individual crystals were at least 80% complete to 2-Å resolution with R_{sym} = 5.5%–7.5%.

Model Refinement. Cubic bovine insulin crystal structures at pH 7 and pH 9 in 0.1 M salt (4) were used as starting models for solving the structures at acid pH in 1 M Na_2SO_4. Atomic coordinates and B-factors were refined in the resolution range 10 Å–2 Å by restrained least-squares minimization (13) using the fast Fourier transform algorithm (14), and models were adjusted using the interactive computer graphics program FRODO (15). Atomic parameters for the ligand and water molecules in the dihaloalkane- and sulfate-binding sites were adjusted separately by phased heavy-atom refinement (16). The dichloroethane-free and dichloroethane-bound crystal structures at pH 6–11 in 0.1–1 M Na_2SO_4 or Na_2CO_3, and at pH 5–5.7 in 1 M Na_2SO_4 were refined to 2-Å resolution with residual R-factors of 16%–18%. Atomic parameters of poorly ordered water molecules in the binding cavity were adjusted further by a real-space comparison of "Data" and "Model" maps (Fig. 2). Laxly ordered atoms contribute very weakly to the high-resolution diffraction data; thus their parameters are poorly defined by the conventional R-factor minimization. Electron density data maps with coefficients $2|F_{obs}| - |F_{calc}|$ and calculated phases showed laxly ordered water molecules with $B \approx 100$ Å^2 as weak features above the noise level. B-factors and coordinates of these water molecules were adjusted by comparing Model maps with the Data maps until reasonable real-space agreement was obtained.

RESULTS AND DISCUSSION

Bound Dichloroethane and Cavity Structure at pH 6–11. Dichloroethane is symmetrically bound across the 2-fold axis in the insulin dimer cavity (Figs. 1, 2*A*, 3*A*, and 4*A*). The cavity is formed by atoms of two copies of B9 serine, B12

The publication costs of this article were defrayed in part by page charge payment. This article must therefore be hereby marked "*advertisement*" in accordance with 18 U.S.C. §1734 solely to indicate this fact.

†To whom reprint requests should be sent at present address: Biophysics Department, Boston University School of Medicine, Boston, MA 02118.
‡Present address: Institute of Molecular Biophysics, Florida State University, Tallahassee, FL 32306-3015.
§The atomic coordinates and structure factors have been deposited in the Protein Data Bank, Chemistry Department, Brookhaven National Laboratory, Upton, NY 11973 (reference 1APH).

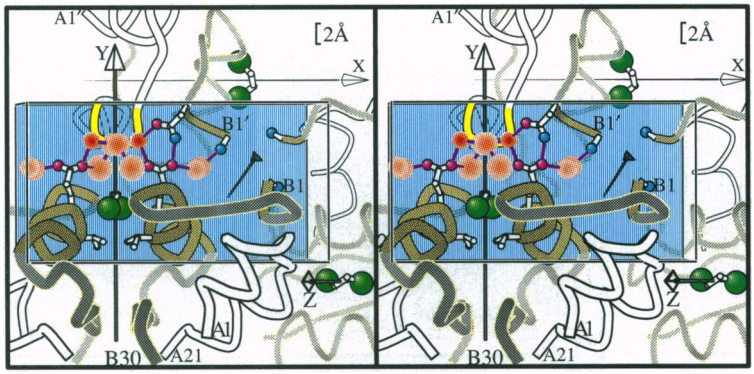

FIG. 1. Cubic insulin crystal packing with bound $ClH_2C—CH_2Cl$. *X*, *Y*, and *Z* mark equivalent orthogonal dyad axes. The MolScript (5) stereoview is normal to *Y* and 17 ± 2° to the right of *Z*. The box, containing one dichloroethane and a trigonal set of B1 α-amino groups, is enlarged and tilted 18° forward in Fig. 3. Shown in the box are cavity-forming residue pairs B12 valine and B13 glutamate, and one copy of B3′ asparagine from the enclosing row of dimers. A-chain is light, and B-chain is shaded; portions in the box are highlighted. Cl, green; O, magenta; N, cyan; water, red Gaussian sphere with radius proportional to rms atomic displacement $\langle u^2\rangle^{1/2} = 1/2\pi(B/2)^{1/2}$; H bonds linking protein and waters are purple.

valine, B13 glutamate, and B16 tyrosine from the dihedrally related α-helical segments B9–B19 and is closed off by portions of the residue pairs A13′ leucine, A14′ tyrosine, and B3′ asparagine from the cross-connected dimer row (parts of which are shown at the top in Figs. 1, 3, and 4). The planar trans-conformation of 1,2-dichloroethane, which constitutes ≈80% of the liquid phase, cannot fit in the cavity. Separate refinement of the chlorine and methylene carbon positions, occupancies, and *B*-factors indicates that at least 70% of the bound dichloroethane is in the staggered right-handed rather than the alternate left-handed cis-conformation. The refined *B*-factors for the Cl and C atoms are, respectively, 32 Å² and 22 Å², which are close to the $\langle B\rangle$ = 22 Å² for all protein atoms.

In the absence of bound ligand, the cavity contains five pairs of water molecules (I–V in Figs. 2*B*, 3*B*, and 4*B*). Dihaloalkane binding displaces two pairs of laxly ordered water molecules IV and V and enhances the ordering of water pair III, as indicated by the decrease in its *B*-factor from 90 Å² to 40 Å². Ligand entry must involve large-amplitude movements of the atoms gating the cavity. Molecular dynamics simulations of the entry of Xe into internal cavities of metmyoglobin (17) have illustrated protein breathing motions in such hydrophobic ligand binding, which involve transient atomic displacements of several Å but no overall change in the cavity structures. Similarly, the refined electron-density maps of the insulin crystals with and without dichloroethane (Fig. 2 *A* and *B*) showed no significant shifts in the atomic positions of the protein and conserved ordered solvent. The rms deviation between the insulin atomic positions in the dichloroethane-free and -bound crystal structures at pH 9 is 0.16 Å for all protein atoms and 0.15 Å for the cavity-forming atoms, and there are no noticeable alterations in any of the protein atomic *B*-factors.

Over the pH range 6–11 at ionic strength 0.1–3 M dichloroethane occupancy remained complete, and the atomic positions of the cavity-forming atoms did not measurably change, as indicated by the refined electron-density maps. However, localized variations do occur in nearby residues, including A5 glutamine, B10 histidine and B25 phenylalanine, which switch their rotamer conformations at particular conditions within this pH and ionic strength range (4).

Structural Transition Between pH 6 and 5.7. An abrupt structural transition occurs when the pH is lowered to 5.7 in 1 M Na_2SO_4, which involves SO_4^{2-} binding and coordinated rearrangement of the cavity-forming residues B13 glutamate, B12 valine and the N-terminal segment B1′–B3′ of the cross-connected molecules. In the dichloroethane-free crystal structure analyzed at pH 5–5.7 (Figs. 2*C*, 3*C*, and 4*C*) compared with that at pH 6–11 (Figs. 2*B*, 3*B*, and 4*B*), B13 glutamate side chains have rotated by ≈120° about χ_1, 25° about χ_2, and 75° about χ_3, which reduces the carboxyl oxygen separation across the dyad from 6.3 Å to 3.6 Å. Half-occupancy of an alternate B12 valine rotomer position, rotated by 120° about χ_1, decreases the accessible volume at the bottom of the cavity. The constriction of the cavity expels two pairs of water molecules, leaving the pair IV, whose *B*-factor has increased from 60 to 80 Å². There is insufficient space inside the rearranged cavity to accommodate a dihaloalkane ligand. Furthermore, the trigonally related B-chain N-termini, which are linked to the B13 carboxyl groups by the discretely disordered water molecules VI at pH 6–11, adopt a new conformation at pH 5–5.7. In this change, the trigonally related B1 α-amino groups, which coordinate three sulfate ions, rotate ≈75° about Ψ, shifting their position by ≈4 Å.

Switching from pH 6 to 5.7 involves cooperative proton binding and rearrangement of the hydrogen-bonded water network interconnecting the B13 carboxyl pairs and the triads of B1 α-amino groups. In the transition from the structure shown in Figs. 3*B* and 4*B* to that in Figs. 3*C* and 4*C*, water molecules I and II shift parallel to their connecting H bond by ≈1 Å. Water molecule I conserves four H bonds, and water molecule II remains connected with A14′N but forms new H bonds to its symmetry mate and to the repositioned B13 Oε2, which displaces water molecule III. The water II pair provides a shuttling conduit for the proton shared by the B13 carboxyl pair. Water molecule III* is located near the former position of B13 Oε2 and is H-bonded to B13 Oε1, B3′N, and water molecule VI which, in turn, is H-bonded to a sulfate oxygen. (At pH 6–11, the discretely disordered water VI H-bonds to either B13 Oε2 or to B1′N.) The well-ordered sulfate at pH 5–5.7, in the absence of dichloroethane, is bound with unit occupancy and is coordinated by five amino groups from the rearranged B1–B3 segments. The oxyanion coordination is similar to that in other proteins (18) and apparently requires complete protonation of B1 NH_3^+ groups.

The conformational changes involved in the transition of cubic insulin at pH 5.7 correlate with structural features observed in different crystalline forms of hexameric insulins. In 2-Zn-insulin crystallized at pH 6.3, the neighboring B13 carboxyl groups are directly connected by a 2.6-Å H bond (19), whereas in the rhombohedral insulin/phenol complex crystallized at pH 8.5, the B13 glutamate residues are turned away from each other (20) as a result of the electrostatic repulsion on deprotonation. In cubic insulin crystals, close apposition of the carboxyl pair at pH ≤ 5.7 in 1 M Na_2SO_4 must enhance the binding of the proton evidently shared through the water II pair. Half-occupancy of the two B12 valine rotamer positions in the low-pH cubic insulin structure corresponds to the two conformations of the asymmetrically related pair of these residues in the rhombohedral 2-Zn-insulin dimer (19). The variety of interactions involving B12 valine and B13 glutamate pairs in insulin dimers in different crystalline forms displays aspects of the conformational adaptability of the monomer that is essential for its receptor-binding activity (21, 22).

Dichloroethane Binding Energy Below and Above pH 5.7. At pH 5–5.5 in the presence of dichloroethane, the refined electron-density maps show an equal mixture of the ligand-bound and ligand-excluding cavity structures, together with half-occupancy of the sulfate-binding site that has the B1

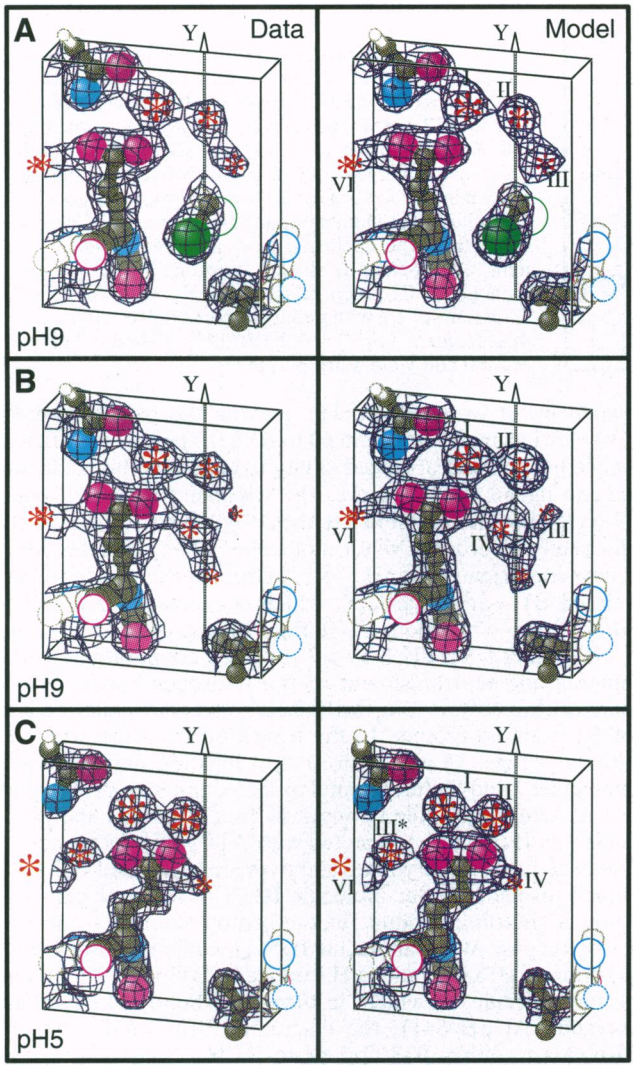

FIG. 2. Electron density of B3′ asparagine, B12 valine, B13 glutamate and solvent in half of the binding cavity: with dichloroethane at pH 9 (*A*), and without dichloroethane at pH 9 (*B*) and pH 5 (*C*). *X*, *Y*, *Z* dimensions of the box are 11 × 13 × 4 Å with the dyad *Y* axis in back (oriented as in Fig. 3). "Data" maps were computed with model-phased coefficients $2|F_{obs}| - |F_{calc}|$, and "Model" maps with F_{calc} using only terms corresponding to the F_{obs} in the resolution range 10–2 Å. Sizes of asterisks marking waters are inversely proportional to the rms displacements. Roman numerals label waters as in Fig. 3. Without the low-resolution data, water molecules with large temperature factors appear as weak features, which are shown by the model simulations to be above noise level. Water *B*-factors range from 20 Å^2 for water molecules I and II in *C* to 90 Å^2 for water molecule III in *B*. Electron density maps were derived from FRODO (15) output files.

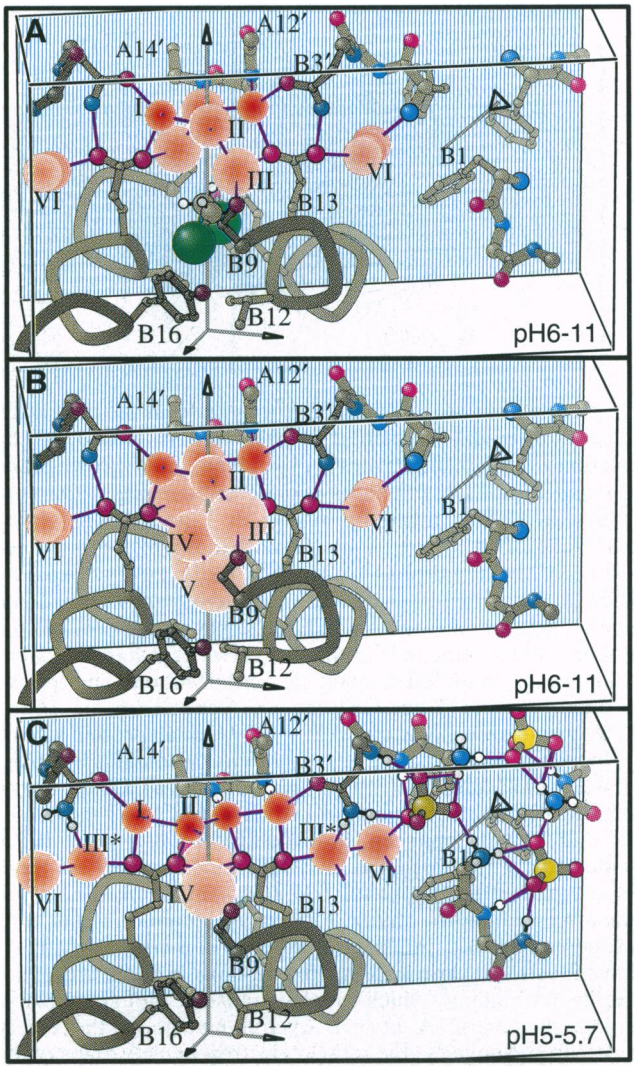

FIG. 3. Interactions in the pH-sensitive dyad cavity with $ClH_2C—CH_2Cl$ at pH 6–11 (*A*) and without $ClH_2C—CH_2Cl$ at pH 6–11 (*B*) and pH 5–5.7 (*C*). The box includes B1′–B3′ (FVN), B9–B16 (SHLVEALY) and one copy of A12′–A14′ (SLY) (illustrated side chains are indicated by underlined boldface type). Water molecules (red Gaussian spheres) are labeled with Roman numerals. Corresponding labels are kept fixed to reference the positions of protein residues and water molecules (except label II in *C*). Between *A* and *B*, there are no significant shifts in the positions of protein atoms and conserved waters. In *C*, the cavity is constricted, and SO_4^{2-} ions H-bond to nitrogens in the triad of N-terminal segments B1–B3; white spheres mark inferred positions of protons attached to nitrogens. H bonds (purple lines) between water molecules are 2.6–3.0 Å long and H bonds between SO_4^{2-} and nitrogens are 2.8–3.4 Å long.

NH_3^+ group in its low-pH conformation. Because the dichloroethane concentration in the saturated solution is ≈0.1 M, the binding constant at pH ≤ 5.7 is ≈10 M^{-1}. Ligand was completely removed from an x-ray-analyzed crystal by washing with five changes of a 100-fold excess of the pH 5 buffer over a 48-hr period. In contrast, similar washings of two crystals at pH 9 did not reduce the dichloroethane occupancy measured from the difference density maps. A change of >3 electrons at a localized site will produce a measurable peak in a 2-Å resolution difference map of these crystals (3), implying that a decrease in chlorine occupancy by >20% should have been detected. Therefore, the observed flat difference map after five washings with a 100-fold excess of pH 9 buffer sets a lower limit for the binding constant of ≈10^5 M^{-1} if equilibrium was attained at each buffer change. Assuming that the interaction energy of the ligand with the protein atoms forming the cavity is independent of pH, the energy required to expand the cavity to the accommodating size at pH 5–5.7 with concomitant displacement of the neighboring sulfate ions should be comparable to the difference between the overall free energy of dichloroethane binding at pH 5 and pH 9. From the results of the washing experiments, the difference in the conformational energy of the expanded compared with the constricted cavity structure at pH < 5.7 is estimated to be >5 kcal/mol.

Ligation of Dichloroethane. High-affinity binding of *cis*-dichloroethane in the pH 9 crystal structure can be accounted for by the snug van der Waals fit in the preformed cavity and

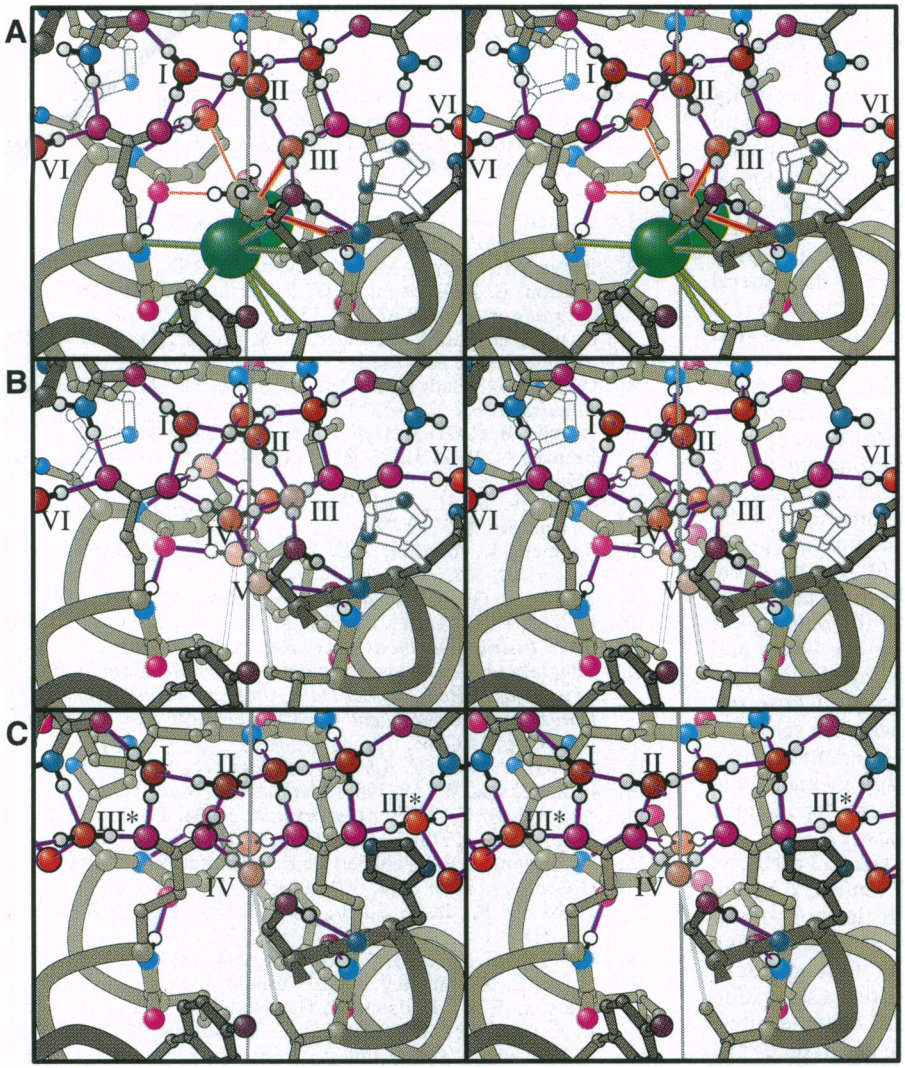

FIG. 4. Water hydrogen bonding and specific contacts with dichloroethane in the dyad-binding cavity. Stereoviews with the same orientation and cavity-forming residue pairs as Fig. 3, plus B10 histidine and single copies of A13′ leucine and A14′ tyrosine. In *A* and *B* at pH 6–11, two conformations of B10 histidine occur: the light one is favored at lower pH. Water oxygens with temperature factors of ≈20 Å^2 are red; those that are more disordered are more lightly shaded. The inferred proton positions (white spheres) form a self-consistent set of H bonds (purple lines). Nine of the ten H bonds formed by the four unique water molecules in *A*, fourteen of the fifteen H-bonds formed by the six water molecules in *B*, and the thirteen H bonds formed by the five water molecules in *C* range in length from 2.6 to 2.9 Å with a mean of 2.7 Å; the H bond from water molecule III to B9 Oγ in *A* and *B* is 3.3 Å. The pentagonal H-bonded rings resemble water clathrate structures. In *C* at pH 5–5.7, the water II pair acts as a conductor for the proton shared by the B13 carboxyl pair. In *A*, contacts between chlorine and its six nearest neighbors (green lines) are 3.7 Å to B12 Cγ and B13 Cα, 3.9 Å to B9 Cβ, and 4.0 Å to the three other carbons. The ligand methylene carbon short contacts (red lines) are 3.1 Å to water molecule III and 3.6 Å to B9 O. The distance from the B12 Cγ at the bottom of the cavity to the nearest water (gray lines) is 3.8 Å in *B* and 5.4 Å in *C* from the valine with the alternate rotamer conformation. POSTSCRIPT code from the MolScript program (5) used for the figures was modified to include highlights, enhance depth cueing, and produce Gaussian spheres of radii proportional to the rms displacements.

the favorable electrostatic interactions (Figs. 3*A* and 4*A*). Each chlorine atom is within 3.7–4.4 Å of 12 neighboring protein carbons, 2 oxygens (4.1 and 4.3 Å away), and 1 nitrogen (4.1 Å); the mean separation between chlorine and its six nearest neighbors (all carbons) is 3.9 Å, which is close to the expected van der Waals contact of 3.8 Å. The ligand dipole is aligned by electrostatic interaction with the pair of carboxylate anions and the negative poles of the water III pair that are oriented by H-bonding to the B13 carboxylates, B9 serine hydroxyl oxygens, and water II protons, as illustrated in Fig. 4*A*. Furthermore, the right-handed *cis*-dichloroethane conformation may be stabilized by interactions of the electropositive methylene carbons with the nearby electronegative oxygens of B9 and water III, which are, respectively, 3.6 Å and 3.1 Å distant. The left-handed conformation, in which the methylene carbons would be shifted by ≈1 Å about the dyad, is sterically allowed but appears energetically less favored because of increased separation from the electronegative oxygens. The estimate from the refined electron-density maps that at least 70% of the dichloroethane is in the right-handed cis-conformation indicates a minimal preference in the binding energy of ≈0.6 kcal/mol for the right-handed compared with the left-handed rotamer.

Selectivity of Haloalkane Binding. Other dihaloalkanes that bind with high occupancy in the same position as *cis*-1,2-dichloroethane (van der Waals end-to-end length L = 7.2 Å) include *cis*-1-bromo,2-fluoroethane ($BrH_2C—CH_2F$, L = 6.9 Å), dibromomethane ($BrCH_2Br$, L = 7.1 Å), iodochloromethane (ICH_2Cl, L = 7.2 Å), and *cis*-1,2-dibromoethylene (BrHC=CHBr, L = 7.4 Å). Bromofluoroethane, the shortest of these ligands, binds relatively weakly, as demonstrated by its complete displacement after a single washing with a 100-fold excess of pH 9 buffer. Reduced affinity of the cavity for dibromoethylene, which is the largest ligand found to bind from saturated solutions, was indicated by its refined occupancy of only ≈70%.

Lack of binding of larger dihaloalkanes, such as *cis*-1,2-dibromoethane ($BrH_2C—CH_2Br$, L = 7.7 Å), can be accounted for by the steric restraints of the tight cavity. Failure of *cis*-1,2-dichloroethylene (ClHC=CHCl, L = 6.9 Å) to bind was unexpected, because it is chemically homologous to BrHC=CHBr and should fit as well as $BrH_2C—CH_2F$, which has the same length. However, with the halogen atoms in corresponding cis-positions, the electropositive carbons of an ethylene compound, unlike those of the right-handed ethane ligands, cannot make the close electrostatic connection with the B9 and water III oxygens. Binding of dibromo- but not dichloroethylene can be attributed to the greater polarizability of Br, which would enhance the dispersion interactions. As expected, no binding was observed with the smaller haloalkanes, dichloromethane ($ClCH_2Cl$, L = 6.5 Å) and iodoethane ($IH_2C—CH_3$, L = 6.6 Å) or with the bulky compounds, chloroform ($CHCl_3$) and halothane ($BrClHC—CF_3$).

Hydrophobic Ligand Binding. Volatile halogenated hydrocarbons are common general anesthetics. The dihaloalkane-binding site in cubic insulin has properties in common with those inferred for anesthetic-binding sites in sensitive protein

targets (6, 7), as well as with the substrate-binding site of haloalkane dehalogenase (23). An amphiphatic pocket that can accommodate polarizable hydrophobic ligands is characteristic of these sites. The dehalogenase has high specificity for the halogen end of its substrate but can accommodate ligands of different sizes. The size-selectivity of the insulin dimer cavity is similar to the "cutoff effect" in the action of general anesthetics: in a homologous series of general anesthetics, the potency increases with increase in the molecular size until a critical size when the potency suddenly disappears (24). Differential action of enantiomers of the general anesthetic isoflurane on neuron ion channel conductivity (25) implies binding-site stereoselectivity comparable with that displayed by the cubic insulin cavity.

Binding of selected dihaloalkanes by cubic insulin must have a large favorable enthalpic contribution because the entropy change for transfer of all the sterically acceptable hydrophobic ligands from the aqueous environment to the invariant cavity should be comparable. Similar enthalpically favored hydrophobic bonding has been demonstrated in the formation of cyclophane–arene inclusion complexes stabilized by strong host–guest interactions (26). In the cubic insulin–dihaloalkane complexes, both dispersion and polar interactions must contribute significantly to the binding enthalpy and stereospecificity. Polarization of the water and protein structure appears critical in mediating the electrostatic interactions with the hydrophobic ligand, whose polarity will be enhanced by the interactions with the selective polar environment. Similar types of polar interactions may account for the significant negative enthalpy in anesthetic binding indicated by the observed temperature dependence of the potency of various general anesthetics (27).

Carboxyl Pairing. The close apposition of the B13 carboxyl groups in cubic insulin crystals at pH 5–5.7, enforced by the water-linked electrostatic interactions with the bound sulfates, enhances the proton binding that drives the cooperative structural transition. Carboxyl pairing can function as a sensitive electrostatic switch to control protein association and can polarize bound water in catalytic enzyme sites. Association of tobacco mosaic virus protein is driven by the cooperative protonation of carboxyl pairs with $pK \approx 7$, which are held together by the packing restraints in the helical assembly (28, 29). The closely paired active-site carboxyl groups in aspartic proteinases, which share a proton linked by the central bound catalytic water, are constrained together by a network of protein and water H bonds (30). In all these structures, the favored binding of a single proton by paired carboxyl groups results from their close apposition imposed by stabilizing interactions elsewhere in the structure.

Allosteric Switching. Binding of dichloroethane in the cubic insulin dyad cavity at pH 5–5.5 requires switching of the B13 carboxyl groups from their closely apposed to their separated, high-pH conformation, with concomitant displacement of the neighboring sulfates which are 13 Å distant from the cavity center. This allosteric effect may be mechanistically similar to the antisickling action of dichloromethane, which has been attributed to a local conformational change at one of the binding sites in deoxyhemoglobin (31). Linkage between dichloroethane and sulfate binding at the spatially remote sites in cubic insulin illustrates how volatile anesthetics may act on sensitive protein targets in the nervous system as allosteric effectors (6).

We thank Dr. Youli Li for help with the x-ray data collection and Dr. John Badger for useful discussions. This work was supported by National Institutes of Health Grant CA-47439 from the National Cancer Institute to D.L.D.C.

1. Dodson, E. J., Dodson, G. G., Lewitova, A. & Sabesan, M. (1978) *J. Mol. Biol.* **125,** 387–396.
2. Badger, J., Harris, M. R., Reynolds, C. D., Evans, A. C., Dodson, E. J., Dodson, G. G. & North, A. C. T. (1991) *Acta Crystallogr. Sect. B* **47,** 127–136.
3. Gursky, O., Li, Y., Badger, J. & Caspar, D. L. D. (1992) *Biophys. J.* **61,** 604–611.
4. Gursky, O., Badger, J., Li, Y. & Caspar, D. L. D. (1992) *Biophys. J.* **63,** 1210–1220.
5. Kraulis, P. (1991) *J. Appl. Crystallogr.* **24,** 946–950.
6. Franks, N. P. & Lieb, W. R. (1994) *Nature (London)* **367,** 607–614.
7. Abraham, M. H., Lieb, W. R. & Franks, N. P. (1991) *J. Pharm. Sci.* **80,** 719–724.
8. Rayment, I., Johnson, J. E. & Suck, D. (1977) *J. Appl. Crystallogr.* **10,** 365.
9. Kalata, K. (1985) *Methods Enzymol.* **114,** 486–510.
10. Phillips, W. C., Li, Y., Stanton, M., Xie, J. & Kalata, K. (1993) *Nucl. Instrum. Methods Phys. Res.* **A334,** 621–630.
11. Pflugrath, J. W. & Messerschmidt, A. (1987) *Computational Aspects of Protein Crystal Data Analyses: Proceedings of the Daresbury Study Weekend* (Fast System Software, Daresbury, U.K.), pp. 149–161.
12. Kabsh, W. (1988) *J. Appl. Crystallogr.* **21,** 916–924.
13. Hendrickson, W. A. (1985) *Methods Enzymol.* **115,** 252–270.
14. Agarwal, R. C. (1978) *Acta Crystallogr.* **34,** 791–809.
15. Jones, T. A. (1978) *J. Appl. Crystallogr.* **11,** 268–272.
16. Dickerson, R. E., Weinzierl, J. E. & Palmer, R. A. (1968) *Acta Crystallogr. Sect. B* **24,** 997–1003.
17. Tilton, R. F., Jr. & Singh, U. C. (1988) *J. Mol. Biol.* **199,** 195–211.
18. Chakrabarti, P. (1993) *J. Mol. Biol.* **234,** 463–482.
19. Baker, E. N., Blundell, T. L., Cutfield, J. F., Cutfield, S. M., Dodson, E. J., Dodson, G. G., Hodgkin, D. C., Hubbard, R. E., Isaacs, N. W., Reynolds, C. D., Sakabe, K., Sakabe, N. & Vijayan, N. (1988) *Philos. Trans. R. Soc. London B* **319,** 365–456.
20. Smith, G. D. & Dodson, G. G. (1992) *Proteins* **14,** 401–408.
21. Derewenda, U., Derewenda, Z., Dodson, E. J., Dodson, G. G., Bing, X. & Markussen, J. (1991) *J. Mol. Biol.* **220,** 425–433.
22. Hua, Q. H., Shoelson, S. E., Kochoyan, M. & Weiss, M. A. (1991) *Nature (London)* **354,** 238–241.
23. Verschueren, K. H. G., Seljee, F., Rozenboom, H. J., Kalk, K. H. & Dijkstra, B. W. (1993) *Nature (London)* **363,** 693–698.
24. Franks, N. P. & Lieb, W. R. (1985) *Nature (London)* **316,** 349–351.
25. Franks, N. P. & Lieb, W. R. (1991) *Science* **254,** 427–430.
26. Smithrud, D. B., Wyman, T. B. & Diedrich, F. (1991) *J. Am. Chem. Soc.* **113,** 5420–5426.
27. Dickinson, R., Franks, N. P. & Lieb, W. R. (1993) *Biophys. J.* **64,** 1264–1271.
28. Caspar, D. L. D. (1963) *Adv. Protein Chem.* **18,** 37–118.
29. Namba, K. & Stubbs, G. (1986) *Science* **231,** 1401–1406.
30. Davies, D. R. (1990) *Annu. Rev. Biophys. Biophys. Chem.* **19,** 189–215.
31. Schoenborn, B. P. (1976) *Proc. Natl. Acad. Sci. USA* **73,** 4195–4199.